Bidirectional Vehicle-to-Grid Interface under a Microgrid Project

Vicente Leite[1, 2], Ângela Ferreira[1, 2], José Batista[1]
[1] Polytechnic Institute of Bragança
Bragança, Portugal
{avtl, apf, jbatista}@ipb.pt
[2] CISE - Electromechatronic Systems Research Centre
UBI, Covilhã, Portugal

***Abstract*—In the emergent deployment of the smart grids, storage systems play an important role into assets utilization optimization, providing backup power and peak-shaving. This concept becomes more critical in the context of microgrids with a high penetration of renewable energy resources. Plug-in electric vehicles provide an enormous distributed storage capability, which favours the technical and economical exploitation of such systems. This paper presents a comprehensive implementation and control of a bidirectional power converter for vehicle-to-grid integration, based on a bidirectional DC/DC converter followed by a full bridge DC/AC converter. The evaluation of the adopted topology and its control is performed through simulation and experimental validation.**

Keywords— Batteries; Converters; Distributed Generation; Energy storage; Grid-to-Vehicle; Microgrids; Vehicle-to-Grid.

I. INTRODUCTION

Considering both existing policies and declared intentions by countries, world primary energy demand is projected to increase by 1,2% per year, on average, from now until 2035. Electricity demand is projected to grow by a higher rate, 2,2% per year, considering it is expected that applications, formerly based on chemical energy, will be based on electrical energy in the following decades [1]. Additionally, the need for dependency reduction on imported fossil fuels and decarbonised electricity have arisen and a sustainable energy system is on the agenda. Electricity, heat generation and transport are the three major consumers of fossil fuel [2-4]. These sectors were responsible for nearly two-thirds of global CO_2 emissions in 2009 [5]. The first two sectors were responsible for 41% of the world CO_2 emissions while the transport sector was responsible for 23% [5]. In accordance with the report from E3G with the Climate Change Group [6], the emissions in this sector are projected to increase by 84% in 2030. Furthermore, the long-lasting instability in many fossil fuel-producing countries increases the price of energy and reinforces the need to find alternatives. As a consequence, a paradigm shift has arisen in the global energy sector, foreseeing a sustainable and environmentally friendlier development [7].

There is not a single solution for the problem of energy in the World, but an increasing utilization of distributed energy resources (DER), mainly based on renewable energy sources (RES) allowing the organization of the energy infrastructure into microgrids, can give a very important contribution to it. A microgrid is a local grid integrating DER, energy storage devices and dispersed loads, which may operate in utility grid connected mode, enhancing the power generation capability, or in islanded mode, allowing a reduction of the actual stress of the transmission power systems and contributing to the electrification of remote areas [8, 9].

Another significant contribution to the new paradigm in the energy sector is the deployment of electric propulsion systems, replacing internal combustion engine (ICE) vehicles by plug-in electric vehicles (PEV), hybrid and also fuel-cell vehicles, with similar driven performance, better efficiency, passenger comfort and safety [7, 10, 11]. Thus, more and more companies are focusing in vehicles driven by electrical propulsion systems [7, 12] as well as governments and customers [13]. Based on moderate expectations, up to 35% of the total vehicles in the U.S. will be PEV or hybrid vehicles by 2020 [14]. It is a matter of fact that we are witnessing a widespread dissemination of light electric vehicles with enormous advantages in the urban areas [15] and, as predicted in [12], by 2030 in the U.S., electric car sales will account for 64% of the light vehicle sales and comprise 24% of the light vehicle fleet. Moreover, these new vehicles have an enormous distributed energy storage capability with an attractive potential of integration with the electrical grid providing optimization of the assets utilization, smoothing the output and variability of RES, by acting as a manageable backup power device and discharging energy back to the grid when necessary, in a grid-to-vehicle (G2V) and vehicle-to-grid (V2G) concept, respectively, engendering the G2V/G2V interface technologies [2-4, 11, 16].

This paper presents a bidirectional power converter topology and the implemented control strategy, for the integration of the battery of an electric vehicle in a small microgrid which has been developed as a research platform and also for demonstration purposes in the context of an university campus [17]. The electric vehicle is called IPB ECO Buggy [18] and it was developed for demonstration purposes and widespread dissemination of electric vehicles.

978-1-4799-2147-8/14/$31.00 ©2014 IEEE

The IPB microgrid and the IPB ECO Buggy are described in Section 2 and the bidirectional power topology for G2V/V2G integration, as well as the control strategy are described in Section 3. In section 4 the simulation results and preliminary experimental results are presented. Finally, there are drawn the main conclusions of the paper.

II. Description of the Microgrid

The IPB microgrid has been developed as a research platform and also for demonstration purposes in the context of an university campus, as part of a wider project named VERCampus – Live Campus of Renewable Energies – which integrates a set of technologies, infrastructures, and initiatives carried out in the university Campus of the Polytechnic Institute of Bragança (IPB). The main purpose of this project is the promotion of DER with integration of renewable energies technologies, for IPB students, stakeholders and all community in general [17, 19].

Another interesting infrastructure to be integrated with the microgrid is the electric vehicle IPB ECO Buggy developed using state-of-the-art technology including a lithium battery [18], as described below.

A. The IPB Microgrid Project

The IPB microgrid has been developed for isolated and self-sustainable systems up to a rated power of 5 kW integrating RES with the purpose of being a demonstration platform in terms of technology transfer and applied research.

The microgrid uses a bidirectional inverter Sunny Island, from SMA, which is the core equipment responsible for the management of the energy flow, and incorporates the following DER: a small 1,4 kWp wind turbine; a solar tracker with a 3 kWp photovoltaic (PV) string; a 2 kWp PV string installed on the roof of the laboratory; a 5 kW back-up diesel generator, powered by a mix with 40% of biodiesel produced from wasted oils in the biofuels laboratory and a 200 Ah battery bank.

A pico run-of-river hydropower plant with 1 kWp and a 1,34 Wp photovoltaic glass facade are also under development and will be integrated into the microgrid in the foreseeable future [20].

B. The IPB ECO Buggy

The IPB ECO Buggy [18] is a light electric vehicle using state-of-the-art technology with respect to the electric propulsion system. Its battery is to be integrated into the microgrid as an additional energy storage element. A lithium iron phosphate battery was chosen for the IPB ECO Buggy due to its advantages. Indeed, nowadays, lithium iron phosphate ($LiFePO_4$) has been investigated intensively [21, 22] as a potential cathode material for rechargeable lithium ion batteries due to the low cost of raw materials, long life cycle and superior safety characteristics [21, 23]. Table I shows the main specifications of the battery.

A likely scenario in the context of smart grids, for storage-grid interaction is the integration of electric vehicles, PEV and fuel-cells, which provide an enormous distributed energy storage capability, allowing the optimization of the assets utilization, acting as a manageable load and discharging energy back to the grid when necessary. This potential is especially important under the context of microgrids with an high penetration of RES: this additional storage capability may be used to smooth the intermittency and variability of most RES and provide a balance in system cost for grid-integrated storage systems. In fact, energy storage may enhance the exploitation of RES, improving the payback period.

TABLE I. Technical Specifications of the $LiFePO_4$ Battery

Voltage	96 V
Capacity	70 Ah (6,5 kWh)
Weight	90 kg
Charging voltage	109,5 V
Discharging limit	75 V
Max. charging/discharging current	140 A

III. Bidirectional Power Topology for V2G/G2V Integration

The converter topology is based on a bidirectional DC/DC converter followed by a full bridge DC/AC converter. The first works as a buck converter for charging the battery (G2V mode) and as a boost converter for injecting current into the grid (V2G mode). The second is a vector controlled single-phase voltage source inverter (VSI).

The converter topology and the basic control schemes are shown in Fig. 1. The shadowed area in Fig. 1 (a) represents an integrated power module from Powerex that is being used in the laboratory platform to implement the V2G/G2V interface. In this case the first leg is used to implement the DC/DC converter and the second and third legs are used as a single-phase VSI.

A. Control of the DC/DC Converter

For the control of the DC/DC converter in V2G mode (discharging mode) the IGBT 1 is always turned OFF and the IGBT 2 is turned ON and OFF at the switching frequency. The IGBT 2, the inductor L and the diode 1 (of IGBT 1) operate as a boost converter. The reference current, $I^*_{b,V2G}$, is set according to the power to be injected into the grid and the maximum admissible depth of discharge.

On the other hand, to control the DC/DC converter in G2V mode (charging mode), the IGBT 2 is always turned OFF and the IGBT 1 is turned ON and OFF at the switching frequency. The IGBT 1, the inductor L, the capacitor C and the diode 2 (of IGBT 2) operate as a buck converter. In this case, the reference current, $I^*_{b,G2V}$, and the reference battery voltage, are set according to a three-stage charge curve defined by the battery manufacturer.

Adopting the generator reference-arrow system, current and power delivered by the battery are positive, *i.e.,* in V2G mode and if the battery is charging, those quantities are negative (G2V mode).

A PI current controller compares the reference current with the measured one, I_b, and generates the control signal for pulse generation (Fig. 1 (b)).

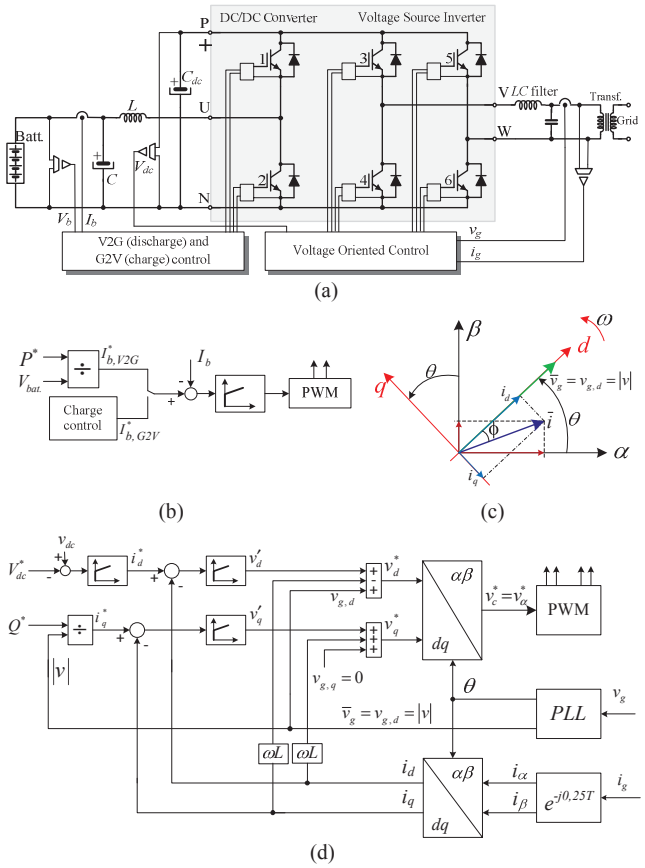

Fig. 1. Converter topology (a) and control schemes: (b) V2G (discharge) and G2V (charge) control; (c) Voltage oriented control of the VSI; (d) VOC scheme.

B. Control of the Voltage Source Inverter

The control scheme of the VSI is shown in Fig. 1 (d) and it is based on the Voltage Oriented Control (VOC) applied to three-phase systems. Three-phase quantities such as grid voltages and currents can be represented by their space phasors which are vectors with two components described in a fixed orthogonal $\alpha\beta$ system. In single-phase systems, the use of such representation is not possible unless a virtual orthogonal component is coupled to the real axis in order to emulate a two axis reference frame. For this purpose, an additional orthogonal component was proposed in [24] by introducing the imaginary orthogonal circuit concept. Thus, auxiliary orthogonal components are obtained by applying a 90º phase shift with respect to their counterparts in the real circuit. Hence, voltages and currents can be represented by their space phasors:

$$\begin{cases} \overline{v}_{\alpha\beta} = v_\alpha + jv_\beta \\ \overline{i}_{\alpha\beta} = i_\alpha + ji_\beta \end{cases} \tag{1}$$

From the output *LC* filter of Fig. 1 (d), and applying Kirchhoff's voltage law,

$$\overline{v}_{c,\alpha\beta} = \overline{v}_{g,\alpha\beta} + R\overline{i}_{\alpha\beta} + L\,d\overline{i}_{\alpha\beta}/dt \tag{2}$$

where R and L are the parasitic resistance and the inductance of the filter, respectively.

The resulting $\alpha\beta$ components are 90º phase shifted sinusoidal signals that can be used for the control of the VSI using classical PI controllers. However, two well-known drawbacks appear: the inability of PI controllers to track sinusoidal references without steady-state error and poor disturbance rejection capability [25]. This occurs due to the poor performance of the integral action if the disturbance is a periodic signal. To overcome these drawbacks of PI controllers with a sinusoidal reference and harmonic disturbances, the power control of the VSI can be implemented in a dq reference frame rotating at an angular speed $\omega = 2\pi f$, where f is the grid frequency. In this so-called synchronous reference frame, the orthogonal components of the grid voltage and current space phasors are DC quantities and, therefore, classical PI controllers can be used since they achieve zero steady state error at the fundamental frequency and improve their dynamic response.

VOC is based on the use of this synchronous reference frame with the dq axes rotating at ω speed and oriented such that the d axis is aligned with the grid voltage phasor as drawn in Fig. 1 (c). By doing this, the quadrature component of the grid voltage will be zero and, consequently, active and reactive powers can be controlled separately by controlling, respectively, the d and q components of the grid current as presented hereinafter.

Considering the rotating transformation of a general variable $\overline{x}$, given by $\overline{x}_{\alpha\beta} = \overline{x}_{dq}e^{j\theta} = \overline{x}_{dq}e^{j\omega t}$, where $\theta = \omega t$ is the angle of the rotating reference frame with respect to the fixed $\alpha\beta$ axes, and replacing (1) into (2), after simple mathematical manipulations the following equations are obtained:

$$\begin{cases} v_{c,d} = Ri_d + L\,di_d/dt - \omega Li_q + v_{g,d} \\ v_{c,q} = Ri_q + L\,di_q/dt - \omega Li_d + v_{g,q} \end{cases} \tag{3}$$

From Fig. 1 (c) and aligning the d axis with the grid voltage phasor results that $v_{g,q} = 0$, from which (3) becomes

$$\begin{cases} v_{c,d} = v'_d - \omega Li_q + v_{g,d} \\ v_{c,q} = v'_d - \omega Li_d \end{cases} \tag{4}$$

where

$$\begin{cases} v'_d = Ri_d + L\,di_d/dt \\ v'_q = Ri_q + L\,di_q/dt \end{cases} \tag{5}$$

In the VOC scheme depicted in Fig. 1 (d), the reference

grid current is composed by two terms: i_d^* and i_q^*. The first one is used to perform the DC-link voltage control and the second one is used to control the reactive power in an independent way. Typically, i_q^* is managed to obtain unity power factor, though the implemented VOC is prepared for reactive power support to the grid, described as follows.

The power control of the grid VSI is based on the instantaneous power theory [26], where the power can be defined in the synchronous reference frame. Assuming that the *d* axis is perfectly aligned with the grid voltage phasor, *i.e.,* $v_{g,q} = 0$, therefore, active power and reactive power, in single-phase systems, are proportional to i_d and i_q, respectively, as follows [27]:

$$\begin{cases} p = 1/2\left(v_{g,d} i_d + v_{g,q} i_q\right) = 1/2\, v_{g,d} i_d \\ q = 1/2\left(v_{g,q} i_d - v_{g,d} i_q\right) = -1/2\, v_{g,d} i_q \end{cases} \quad (6)$$

From the above equation the *dq* components of the reference current are defined by the active and reactive power reference values:

$$\begin{cases} i_d^* = 2P^* / v_{g,d} = 2P^* / |v| \\ i_q^* = 2Q^* / v_{g,d} = 2Q^* / |v| \end{cases} \quad (7)$$

Concerning the active power control, instead of using (7), the i_d^* component of the grid reference current is given by the PI controller in order to maintain the voltage at DC-link constant. The active power control is performed by the boost converter and the reference value is given by the power to be extracted from the battery, in the V2G operation mode, or by the battery charge control algorithm in G2V mode, as depicted in Fig. 1 (b).

Finally, the VOC scheme of Fig. 1 (d) shows the 90º phase delay block (0,25T - a quarter of the grid period) that creates the virtual quadrature component, allowing the emulation of a two-phase system, and also a PLL block that has been implemented to obtain the angle, θ, of the grid voltage, for reference frame transformation and synchronization purposes. The implemented PLL is a second order generalized integrator [28].

IV. Simulation and Experimental Results

In order to evaluate the control performance of the bidirectional converter for V2G/G2V integration described above, it was performed a simulation validation, using MATLAB/Simulink. As far as the control of the VSI is concerned, preliminary experimental results have been achieved. The experimental setup and obtained results are presented in this section.

A. Simulation Results

The simulated scenario, with an elapsed time of 4 s, considers that the battery is charging during the first 1,5 s (G2V mode) and in the remaining time interval, it is discharging (V2G mode). Concerning the initial state of charge (SoC) of the battery, it is assumed to be equal to 90%. An additional operating condition is introduced around 3 s, where the VSI starts supporting the grid with reactive power.

Fig. 2 shows the voltage and current of the battery during the simulation time span. In G2V mode, the current reference value is set by the charging algorithm which is -10 A. In V2G mode, it is defined by the power to be extracted from the battery which was set to 1000 W giving a reference current of about 10 A for the battery voltage of 99,5 V.

Fig. 3 shows the voltage across the DC link capacitor, C_{dc}. The initial voltage of the capacitor is 400 V and, after an initial transient, the voltage PI controller brings the DC voltage to the reference value. When the power converter changes from G2V to V2G operation mode, then the DC/DC converter changes from "buck" to "boost" operation mode. Consequently, the current changes from about -10 A to 10 A and, therefore, the DC voltage tends to increase dramatically but the voltage PI controller rapidly brings the DC voltage to the reference value once again. This is accomplished because the inverter starts injecting current into the grid, as can be seen in Fig. 4: before reaching 1,5 s, the current is in phase opposition with respect to the voltage and after 1,5 s it is in phase. Thus, firstly the power flows from the grid to the battery (negative power) and afterwards from the battery to the grid (positive power). The change from G2V to V2G does

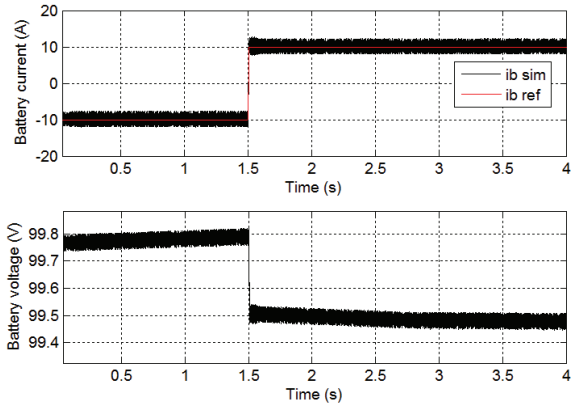

Fig. 2. Battery current (above) and voltage (below).

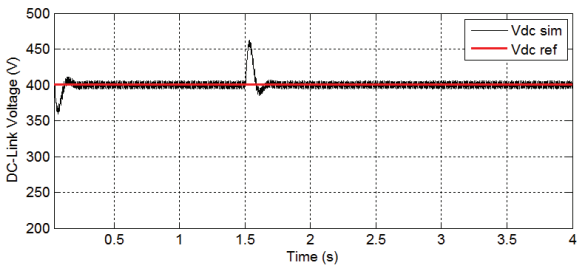

Fig. 3. Voltage across the DC-Link capacitor.

not happen at exactly 1,5 s because there is a ramp limiter to avoid a sudden change in the current reference value.

At 3 s (plus 2 ms to avoid the zero crossing of the current for this test) a step of -400 var is set in the reactive power reference and, therefore, the grid current is not anymore in phase with the voltage and, therefore, the current starts leading the voltage, as can be seen in Fig. 5. This means that the VSI is now delivering reactive power to the grid.

At this time instant, the *q* component of the grid current in the synchronous reference frame changes from 0 to 2,4 A, as can be observed in Fig. 6 (b). The later current value is the one required to inject the specified capacitive reactive power. The evolution of *d* component of the grid current during the simulation time interval is shown in Fig. 6 (a). As expected, this current component does not change when the step of reactive power is introduced but, naturally, the rms value of the grid current increases, in accordance with Fig. 5.

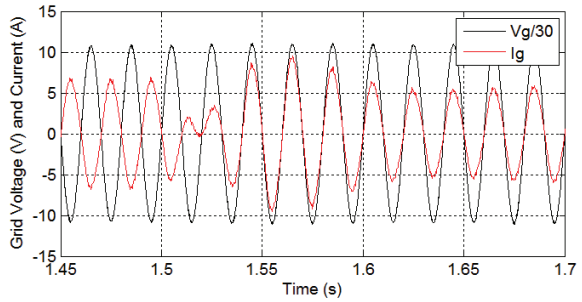

Fig. 4. Grid voltage (scaled) and grid current before and after the change from G2V to V2G mode of operation..

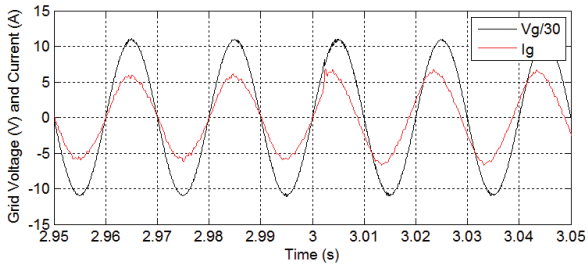

Fig.5. Grid voltage (scaled) and grid current before and after to change the reactive power from 0 to -400 var.

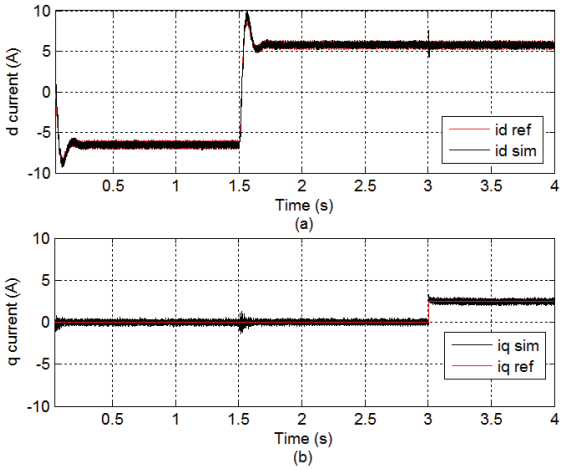

Fig.6. Grid current components in synchronous reference frame: (a) *d* component and (b) *q* component.

B. *Experimental Results*

Preliminary experimental results of the VSI control implementation have already been achieved. The experimental developed setup is based on the MATLAB with Simulink and the dSPACE ACE kit based on the 1103 controller board. The VSI was implemented with the intelligent power module (IPM) PM75RLA120 from Powerex. This is a power module with a three-phase 1200 V IGBT VSI plus an IGBT break. The interface circuit BP7B was used for isolation between the IPM and the controller board connector panel. As remarked in the simulation phase, one leg of the IPM was used for the DC/DC converter and the other two legs were used to implement the single-phase VSI.

The DC-Link voltage was achieved by means of a variable three-phase autotransformer and a rectifier bridge with a 1 mF electrolytic capacitor.

Fig. 7 shows the measured grid voltage and the PLL output. As can be seen, in spite of the grid voltage distortion the PLL extracts perfectly the fundamental component. Fig. 8 shows the *dq* components of the grid current when a step of 400 W is applied, from 800 W to 1200 W. The *q* component keeps equal to zero because the reference value of the reactive power was set to zero. The corresponding active and reactive powers, calculated using (6) and (7), are shown in Fig. 9 (a). The measured DC-Link voltage is also plotted in this figure. The measure grid voltage (scaled), the measured grid current and its reference amplitude can be seen in Fig. 9 (b). As expected the grid current is in phase with the voltage, *i.e.*, assuring a unity power factor.

Another test performed consists in the implementation of reactive power compensation. With initial values of the active and reactive power references set to 800 W and 500 var, respectively, it was imposed a step change of -500 var in the reactive power reference, in order to emulate a full power

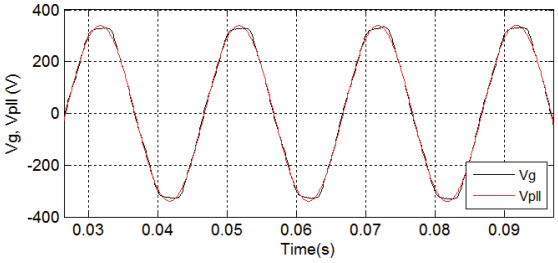

Fig. 7. Grid voltage and PLL output.

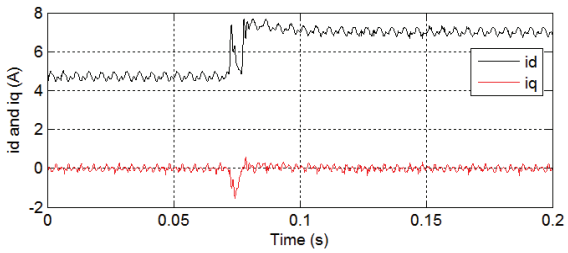

Fig. 8. Grid current *dq* components.

factor correction of the microgrid. Fig. 10 (a) shows the DC-Link voltage and measured active and reactive powers and Fig. 10 (b) plots the grid voltage (scaled), the grid current and the reference amplitude of the grid current. As can be seen from Fig. 10 (b), after the step change, the grid current is in phase with the voltage, while before the current lags the voltage. Thus, VOC can support the microgrid with full reactive power compensation.

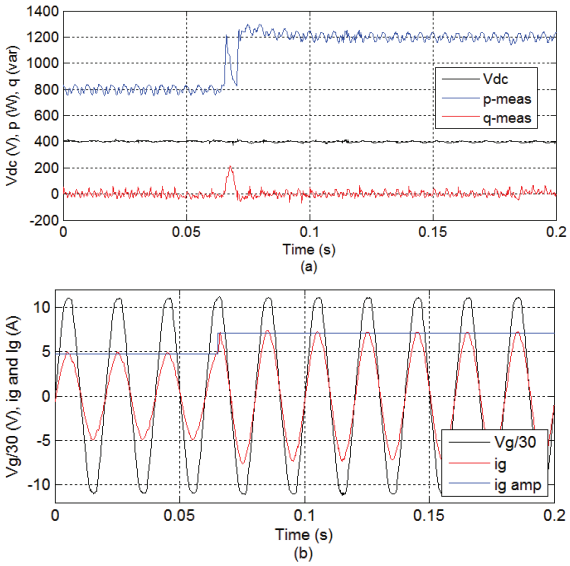

Fig. 9. Application of 400 W step in the active power reference: (a) DC-Link voltage and measured active and reactive powers; (b) grid voltage (scaled), grid current and reference amplitude of the grid current.

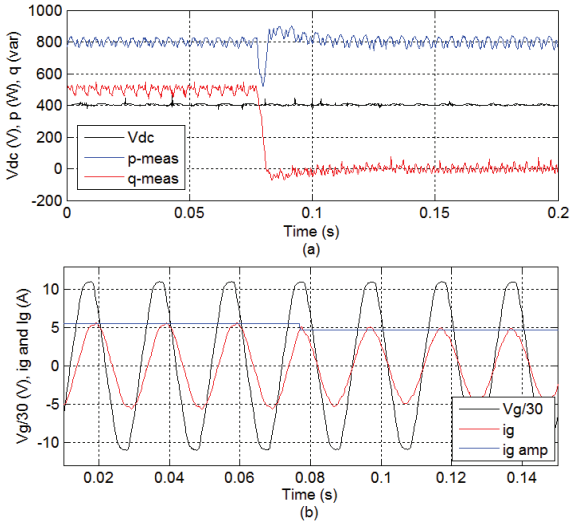

Fig. 10. Application of a -500 var step in the reactive power reference: (a) DC-Link voltage and measured active and reactive powers; (b) grid voltage (scaled), grid current and reference amplitude of the grid current.

V. Conclusions

This paper presented an on-going implementation and validation of a power converter topology for a V2G/G2V interface, for a microgrid project of 5 kW and a light electric vehicle with a lithium ion phosphate battery.

Simulation and experimental results showed that the adopted topology is able to manage bidirectional active and reactive power flow, allowing the battery to behave as an electric load or generator and also to perform power factor compensation of the microgrid.

References

[1] IEA, "World Energy Outlook," International Energy Agency Publications, Technical report. 2012.

[2] M. Ferdowsi, "Plug-in Hybrid Vehicles - A Vision for the Future," in *IEEE Vehicle Power and Propulsion Conference (VPPC 2007)*, Arlington, Texas, 9-12 September, 2007.

[3] A. Y. Saber and G. K. Venayagamoorthy, "One Million Plug-in Electric Vehicles on the Road by 2015," in *12th International IEEE Conference on Intelligent Transportation Systems (ITSC '09)*, St. Louis, MO, 4-7 October, 2009, pp. 1-7.

[4] A. Y. Saber and G. K. Venayagamoorthy, "Plug-in Vehicles and Renewable Energy Sources for Cost and Emission Reductions," *IEEE Transactions on Industrial Electronics,* vol. 58, pp. 1229-1238, April, 2011.

[5] IEA, "CO_2 Emissions from Fuel Combustion – Highlights," in *IEA Statistics*, ed, 2011. Available: http://www.iea.org/co2highlights/CO2highlights.pdf.

[6] S. Tomlinston, "Breaking the climate deadlock: Technology for a low carbon future," ed: E3G with The Climate Group, The Office of Tony Blair, 2008. Available: http://www.tonyblairoffice.org/climatechange/pages/reports/

[7] A. Emadi, L. Young-Joo, and K. Rajashekara, "Power Electronics and Motor Drives in Electric, Hybrid Electric, and Plug-In Hybrid Electric Vehicles," *IEEE Transactions on Industrial Electronics,* vol. 55, pp. 2237-2245, June, 2008.

[8] J. M. Guerrero, P. Loh, T.-L. Lee, and M. Chandorkar, "Advanced Control Architectures for Intelligent Microgrids—Part I: Decentralized and Hierarchical Control," *IEEE Transactions on Industrial Electronics,* vol. 60, pp. 1254 – 1262, April, 2013.

[9] J. M. Guerrero, M. Chandorkar, T.-L. Lee, and P. Loh, "Advanced Control Architectures for Intelligent Microgrids—Part II: Power Quality, Energy Storage, and AC/DC Microgrids," *IEEE Transactions on Industrial Electronics,* vol. 60, pp. 1263 – 1270, April, 2013.

[10] M. Zandi, A. Payman, J. P. Martin, S. Pierfederici, B. Davat, and F. Meibody-Tabar, "Energy Management of a Fuel Cell/Supercapacitor/Battery Power Source for Electric Vehicular Applications," *IEEE Transactions on Vehicular Technology* vol. 60, pp. 433-443, 2011.

[11] F. Zhang and P. Cooke, "The Green Vehicle Trend: Electric, Plug-in hybrid or Hydrogen fuel cell?," Dynamics of Institutions and Markets in Europe (DIME). 2010.

[12] T. Becker, "A New Model with Forecasts to 2030," University of California, Center for Entrepreneurship & Technology (CET), Technical Brief, Number: 2009.1.v.2.0. 2009.

[13] C. C. Chan, "The State of the Art of Electric, Hybrid, and Fuel Cell Vehicles," *Proceedings of the IEEE,* vol. 95, pp. 704-718, 2007.

[14] M. Duvall and E. Knipping, "Environmental assessment of plug-in hybrid electric vehicles. Vol. 1: Nationwide Greenhouse Gas Emissions," EPRI/NRDC, Palo Alto, CA, Final Rep. 1015325. 2007.

[15] M. Bertoluzzo and G. Buja, "Development of Electric Propulsion Systems for Light Electric Vehicles," *IEEE Transactions on Industrial Informatics,* vol. 7, pp. 428-435, 2011.

[16] M. Yilmaz and P. T. Krein, "Review of the Impact of Vehicle-to-Grid Technologies on Distribution Systems and Utility Interfaces," *Power Electronics, IEEE Transactions on,* vol. 28, pp. 5673-5689, 2013.

[17] V. Leite, J. Batista, and O. Rodrigues, "VER*Campus* – Live Park of Renewable Energies," in *International Conference on Renewable*

Energies and Power Quality, ICREPQ, Santiago de Compostela, Spain, 28-30 March, 2012.

[18] V. Leite, J. Batista, J. Lima, and J. Meireles, "The IPB ECO Buggy – A Light Electric Vehicle in a Live Park of Renewable Energies," in *17th International Symposium Power Electronics (Ee2013)* Novi Sad, Republic of Serbia, 30 October-1 November, 2013.

[19] V. Leite, T. Figueiredo, T. Pinheiro, A. Ferreira, and J. Batista, "Dealing with the Very Small: First Steps of a Picohydro Demonstration Project in an University Campus," in *International Conference on Renewable Energies and Power Quality (ICREPQ'12)*, Santiago de Compostela, Spain, 28-30 March, 2012.

[20] V. Leite, A. Ferreira, and J. Batista, "On the Implementation of a Microgrid Project with Renewable Distributed Generation," in *I Congreso Iberoamericano sobre Microrredes con Generación Distribuida de Renovables*, Soria, Spain, 23-24 September, 2013.

[21] A. C.-C. Hua and B. Z.-W. Syue, "Charge and Discharge Characteristics of Lead-Acid Battery and LiFePO4 Battery," in *International Power Electronics Conference (IPEC 2010)*, 21-24 June 2010, pp. 1478-1483.

[22] K. Zaghib, K. Striebel, A. Guerfi, J. Shim, M. Armand, and M. Gauthier, "LiFePO4/polymer/natural graphite: low cost Li-ion batteries," *Electrochimica Acta, ELSEVIER,* vol. 50, pp. 263-270, 2004.

[23] D. Tingting, L. Jun, Z. Fuquan, Y. Yi, and J. Qiqian, "Analysis on the Influence of Measurement Error on State of Charge Estimation of LiFePO4 Power Battery," in *International Conference on Materials for Renewable Energy & Environment (ICMREE 2011)*, Shanghai, 20-22 May, 2011, pp. 644-649.

[24] R. Zhang, M. Cardinal, P. Szczesny, and M. Dame, "A grid Simulator with Control of Single-Phase Power Converters in D-Q Rotating Frame," in *IEEE 33rd Annual Power Electronics Specialists Conference, 2002 (PESC 02)* 23-27 June, 2002, pp. 1431-1436.

[25] R. Teodorescu, M. Liserre, and P. Rodriguez, *Grid Converters for Photovoltaic and Wind Power Systems*: John Wiley & Sons, 2011.

[26] L. S. Czarnecki, "Instantaneous Reactive Power p-q Theory and Power Properties of Three-Phase Systems," *IEEE Transactions on Power Delivery,* vol. 21, pp. 362-367, January 2006.

[27] S. Samerchur, S. Premrudeepreechacharn, Y. Kumsuwun, and K. Higuchi, "Power Control of Single-Phase Voltage Source Inverter for Grid-Connected Photovoltaic Systems," in *Power Systems Conference and Exposition (PSCE), IEEE/PES*, 20-23 March, 2011, pp. 1-6.

[28] M. Ciobotaru, R. Teodorescu, and F. Blaabjerg, "A New Single-Phase PLL Structure Based on Second Order Generalized Integrator," in *37th IEEE Power Electronics Specialists Conference (PESC '06)* 18-22 June, 2006, pp. 1-6.